Soft Matter

Accepted Manuscript

ROYAL SOCIETY OF CHEMISTRY

www.rsc.org/softmatter

Journal Name

ARTICLE TYPE

Cite this: DOI: 10.1039/xxxxxxxxxx

Amphiphilic triblocks to control assembly of mixed or segregated bilayers and monolayers

Christina L. Ting,*[a] Brad H. Jones[a], Amalie L. Frischknecht[b], Erik D. Spoerke[a], and Mark J. Stevens[b]

Received Date
Accepted Date

DOI: 10.1039/xxxxxxxxxx

www.rsc.org/journalname

Triblock amphiphilic molecules composed of three distinct segments provide a large parameter space to obtain self–assembled structures beyond what is achievable with conventional amphiphiles. To obtain a molecular understanding of the thermodynamics of self–assembly, we develop a coarse–grained triblock polymer model and apply self–consistent field theory to investigate the packing mechanism into layer structures. By tuning the structural and interaction asymmetry, we are able to obtain bilayers and monolayers, where the latter may additionally be mixed (symmetric) or segregated (asymmetric). Of particular interest for a variety of applications are the asymmetric monolayers, where segregation of end blocks to opposite surfaces is expected to have important implications for the development of functional nanotubes and vesicles with distinct surface chemistries.

1 Introduction

Amphiphiles, molecules containing discrete solvophilic and solvophobic segments, display exceptional surface activity and a strong propensity to self–assemble in solution over a wide range of environmental conditions. These behaviors are routinely exploited to direct structure formation in complex inorganic materials,[1,2] stabilize colloidal dispersions,[3,4] and compatibilize dissimilar substances for drug delivery[5] and emulsion technology.[6] The most well–studied amphiphiles have distinct solvophilic and solvophobic segments; examples include conventional ionic surfactants, diblock copolymers, lipids, and peptide ampiphiles. Depending on the relative volume fractions of the two segments, these molecules can self–assemble in solution into a variety of structures, such as micelles and bilayers.[7]

Another interesting molecular architecture consists of a solvophobic middle block flanked on both ends by solvophilic groups. This triblock architecture encompasses several well-known classes of amphiphiles, including bolaamphiphiles, where the solvophobic core is typically a lipid-like chain,[8] and triblock polymers,[9,10] bearing chemically identical (copolymer) or distinct (terpolymer) end blocks. The practical significance of these molecules is exemplified by poly(ethylene oxide)-poly(propylene oxide)-poly(ethylene oxide) triblock copolymers,[11,12] sold commercially and used extensively in biotechnological applications,

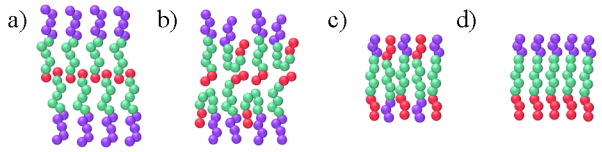

Fig. 1 Schematic of symmetric structures: a) bilayer, b) doubly mixed bilayer, c) mixed monolayer; and asymmetric structures: d) segregated monolayer.

such as gene therapy[13] and drug delivery.[14] Although these applications typically involve the formation of micelles, the triblock architecture has also been exploited for use in a variety of other nanostructures. Ni and Chau recently demonstrated the co-assembly of a virus–like capsid using a peptide amphiphile composed of three distinct segments.[15] Others have used triblock polymers to fabricate solvent–filled nanotubes[16,17] and asymmetric vesicles, where segregation of end blocks to inner and outer surfaces of vesicles has been identified.[18–21]

These nanostructures exploit the ability of the triblock amphiphile to assemble into bilayers and monolayers, as illustrated in Figure 1. For incompatible end blocks, the assembly may additionally be mixed (symmetric) or segregated (asymmetric). The specific packing mechanism preferred by a given triblock amphiphile is dictated principally by the relative volume fractions and interaction strengths between the segments. Depending on the balance of these parameters, other more complex packing modes may occur, such as the doubly mixed bilayer shown in Figure 1b. In contrast, diblock amphiphiles typically self-assemble into only simple bilayers, although segregated bilayers are pos-

[a] *Sandia National Laboratories, Albuquerque, NM 87185, USA. E-mail: clting@sandia.gov*
[b] *Center for Integrated Technologies, Sandia National Laboratories, Albuquerque, NM 87185, USA.*

sible by using mixtures of diblock amphiphiles with solvophilic segments of different size and/or chemistry.[22–29] These mixtures effectively mimic the triblock architecture but the entropy will be different.

Elucidation of the molecular design parameters governing the formation of mixed or segregated forms of monolayers and bilayers is necessary to guide functional use of these amphiphiles. Theory and simulations can provide the desired insights. Cui and Jiang performed Monte Carlo simulations for vesicles composed of monolayers of *ABC* triblock terpolymers. They found that segregation of the ends to the inner or outer surface of the vesicle was dominated by the relative lengths of the end blocks, whereas the dynamics of segregation before or after the closure of the vesicle was determined by the hydrophilicity difference of the end blocks.[30] To complement the simulation work, self–consistent field theory (SCFT) has been used to study the thermodynamics of triblock polymers in dilute solution. Most of these studies involved variations of *ABA* triblock copolymers,[31–33] and we are aware of only one study of a linear *ABC* triblock terpolymer, composed of a relatively short solvophilic *A* block and two solvophobic *B*,*C* blocks.[34] In the present work, we use SCFT to study the assembly of triblock amphiphiles with *ABA* and *ABC*–type architectures, where the *B* block is solvophobic, into bilayers and monolayers, which may additionally be mixed (symmetric) or segregated (asymmetric). Within the large parameter space from which to control the molecular packing of these triblocks, we focus specifically on the effects of asymmetry in the length and interaction strength of the solvophilic end segments.

2 Model and Method

The model consists of amphiphilic triblock polymers (P) in explicit solvent (S). The solvents are modeled as monomers with volume v_S, and the triblocks as polymers, composed of a solvophobic center block (B) flanked by two solvophilic end blocks (A,C), each with monomer volume v_I and block length N_I, where $I = A,B,C$. To understand the effects of changing the relative volume fractions of the two end blocks, we set $N_B = 20$ and vary N_A, N_C while keeping the total chain length $N_P \equiv N_A + N_B + N_C = 32$. For simplicity, all monomer volumes are equal so that the total volume of the triblock is $v_P \equiv vN_P$.

The triblocks are represented as discrete Gaussian chains, where the total bond energy between adjacent monomers at $\mathbf{r}_{i+1}$ and $\mathbf{r}_i$ takes the form

$$h(\{\mathbf{r}\}) = \frac{3k_BT}{2b^2}\sum_i^{N_P-1}(\mathbf{r}_{i+1}-\mathbf{r}_i)^2. \tag{1}$$

In this expression, k_BT is the thermal energy and $b = 0.5$ nm is the bond length. In using the discrete Gaussian chain, local structure and contributions from hydrogen bonding have been neglected. However, the model is general and allows us to focus on how molecular asymmetry can be used to control the thermodynamics of self–assembly. Such simple models of amphiphilic molecules, which allow exploration of conformational space even at a rudimentary level, have made outstanding predictions; see, for example, the HP model by Dill and coworkers.[35]

The essential contributions to the model are the chain connectivity of the triblocks, the short-ranged pairwise interactions between monomer species and the excluded volume effects in an incompressible system. In the grand canonical ensemble, the numbers of molecules are determined from their respective chemical potentials μ_P, μ_S, obtained from the homogenous bulk phase. Following the usual SCF derivation and mean field approximation,[36,37] the field–theoretic grand free energy may be written

$$F = -\frac{e^{\mu_P}}{v_P}Z_P[\xi_A,\xi_B,\xi_C] - \frac{e^{\mu_S}}{v}Z_S[\xi_S] \tag{2}$$
$$+\int d\mathbf{r}\left[\chi_{JK}\phi_J\phi_K + \frac{\kappa_J}{2}|\nabla\phi_J|^2 - \xi_J\phi_J\right].$$

Here, ϕ_J and ξ_J are the volume fraction and conjugate potential fields, respectively, where it is understood that these denote mean fields and we have omitted the $\mathbf{r}$ dependence for notational conciseness. The local and nonlocal interactions are captured by the interaction parameters χ_{JK} and κ_J, respectively, and the double indices represent a sum over monomer species: $J \in \{A,B,C,S\}$ and $JK \in \{AB,BC,AC,AS,BS,CS\}$. In modeling systems involving long polymers, the nonlocal κ_J terms are not usually needed, since the polymer chain connectivity is sufficient to capture nonlocal effects at length scales of interest. Because of the shorter chains in this work, the nonlocal gradient terms are included in the free energy[38], where we set $\kappa_J = 0.35$ for $J = A,B,C$ and $\kappa_S = 0$.

The first line in eq. 2 contains the partition functions for a single molecule in its respective field(s), defined as $Z_S[\xi_S] = \int d\mathbf{r}\exp[-v\xi_S]$ for the solvents and $Z_P[\xi_A,\xi_B,\xi_C] = \int d\mathbf{r}\, q(\mathbf{r},N_P)$ for the triblocks. Here, $q(\mathbf{r},N_P)$ represents the statistical weight for a chain with N_P monomers to have its end monomer at position $\mathbf{r}$. This object is commonly referred to as a chain propagator and will be used to obtain the single–chain statistics of the triblocks; see the Appendix for details. The prefactors before the single molecule partition functions in eq. 2 contain the monomer volume v and the polymer volume v_P, which were used as the volume scales in the total partition function instead of the cube of the de Broglie wavelength. This only shifts the chemical potential and does not affect any of the thermodynamics of interest.

The SCFT equations are obtained by the mean-field approximation, i.e. requiring that eq. 2 is stationary with respect to variations in the fields. Variation with respect to the volume fraction fields ϕ_A, ϕ_B, and ϕ_C gives

$$\xi_A = \xi_S + \chi_{AS}(\phi_S-\phi_A) + (\chi_{AB}-\chi_{BS})\phi_B \tag{3}$$
$$+(\chi_{AC}-\chi_{CS})\phi_C - \kappa_A\nabla^2\phi_A,$$

$$\xi_B = \xi_S + \chi_{BS}(\phi_S-\phi_B) + (\chi_{AB}-\chi_{AS})\phi_A \tag{4}$$
$$+(\chi_{BC}-\chi_{CS})\phi_C - \kappa_B\nabla^2\phi_B,$$

$$\xi_C = \xi_S + \chi_{CS}(\phi_S-\phi_C) + (\chi_{BC}-\chi_{BS})\phi_B \tag{5}$$
$$+(\chi_{AC}-\chi_{AS})\phi_A - \kappa_C\nabla^2\phi_C.$$

Table 1 Range of model parameters

χ_{AC}	χ_{BS}	χ_{AS},χ_{CS}	χ_{AB},χ_{BC}	$\kappa_{A,B,C}$	κ_S	C_P	f_A	N_A	N_B	N_C
$0.0-3.5$	2.5	$0.0-0.25$	2.75	0.35	0.0	1×10^{-5}	$0.08-0.50$	$1-6$	20	$6-11$

Variation with respect to ξ_S gives $\phi_S = e^{\mu_S}e^{-\nu\xi_S}$, which is solved to yield

$$\xi_S = -\frac{1}{\nu}\log[1-\phi_A-\phi_B-\phi_C]. \quad (6)$$

Here the system incompressibility is used to eliminate ϕ_S and to define $\mu_S \equiv 0$ (chemical potentials in an incompressible system are not independent). Variation with respect to ξ_A, ξ_B, and ξ_C gives

$$\phi_I = \frac{ve^{\mu_P}}{v_P}\sum_i q(\mathbf{r},i)e^{\nu\xi_I}q^*(\mathbf{r},N_P-i+1). \quad (7)$$

for $I = A,B,C$. In this expression, the sum runs over the monomer indices i of species I and we have introduced a complementary chain propagator q^*, which propagates from the opposite end of the chain as q. The extra exponential factor cancels out the excess factor of $e^{-\nu\xi_I}$ for joining the two ends. The calculation of the chain propagators for the discrete Gaussian chain is described in the Appendix.

Briefly, the numerical steps to solve the SCFT equations are as follows. First, we begin with a volume fraction field configuration, which satisfies the incompressibility condition $\sum_I \phi_I = 1$ and resembles the structure that we are solving for. Then, eqs. 3–6 are used to obtain the initial conjugate potential fields ξ_I. For a given potential field configuration, the chain propagators are computed from eq. 10 in the Appendix, and input into eq. 7 to obtain the volume fraction fields ϕ_I. Finally, the potential fields are updated by a Picard's method and the iterative scheme repeats. Self-consistency is achieved once the difference in the free energy calculated between iterations reaches an error criterion of 10^{-8}.

3 Bilayers vs. Monolayers

As discussed previously, diblock amphiphilic molecules in solution can self–assemble into a variety of structures. The sheet–like structure typically corresponds to a bilayer, where the solvophilic block forms the outside of both layers and the solvophobic block forms the core of the bilayer. In triblock amphiphiles, the same solvent–driven self–assembly mechanism can lead to the formation of a monolayer, where the solvophilic end blocks form the outside of the monolayer and the solvophobic middle block forms the core. Both of these structures involve a mixture of molecules on both sides and are thus symmetric across the direction normal to the surface of the sheet. However, in triblock amphiphiles, the two end blocks can be incompatible and an additional structure is possible, where the end blocks do not mix and only occur on separate sides of the solvophobic core. This latter structure corresponds to an asymmetric monolayer.

In the grand canonical ensemble the SCFT solutions directly give the preferred packing density and free energy per molecule in an aggregate. By comparing the excess free energy per molecule in the aggregates, we map out the phase diagram as a function of structural asymmetry $f_A = N_A/(N_A+N_C)$ and interaction strength χ_{AC} between the two end blocks. In this work we focus on the following sheet–like structures: bilayers, symmetric monolayers, and asymmetric monolayers. Model parameters are chosen so that layer structures, relative to micelles, are the thermodynamically stable aggregates at experimentally relevant triblock concentrations. This is checked by comparing the excess free energy per molecule in different one dimensional coordinate systems, e.g. cylindrical coordinates for worm-like micelles. Interaction parameters and additional model parameters are summarized in Table 1. Differences in end block compatibility with the solvents (S) and solvophobic monomers (B) are not considered. Hence, $\chi_{AS} = \chi_{CS} = 0$ and $\chi_{AB} = \chi_{BC} = 2.75$, where the latter are chosen to be comparable to χ_{BS}.

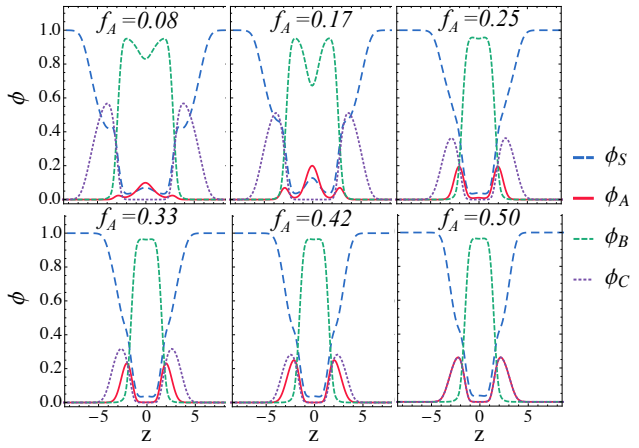

Fig. 2 Volume fraction profiles in the direction z (nm) normal to the sheet, for an ABC triblock with $\chi_{AC} = 0$.

3.1 Effect of structural asymmetry, f_A

In this section, we explore how structural asymmetry affects molecular assembly into bilayers and monolayers. To focus on the architectural effects of the triblocks, an ABC triblock with $\chi_{AC} = 0$ is considered. In our open system, the bulk concentration of triblocks defines the chemical potential. We set the number density of polymers $C_P = 1\times10^{-5}$ nm^{-3} and, as discussed above, have checked that we are working in a concentration regime where the sheet–like structures are thermodynamically preferred over spherical and cylindrical micelles.

Figure 2 shows the $1D$ volume fraction profiles of the molecular aggregates normal to the surface of the sheet, where $z = 0$ corresponds to the center of the sheet. The separate plots show increasing f_A, where the top left figure corresponds to $f_A = 0.08$ and the bottom right figure corresponds to the symmetric case of $f_A = 0.5$. For $f_A \leq 0.17$, the triblocks assemble to form bilayers consisting of a solvophobic B core (green, dashed) lined

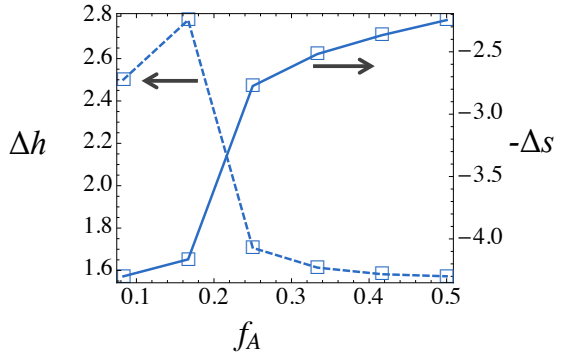

Fig. 3 Enthalpic (dashed) and entropic (solid) contribution to the excess free energy per unit area (k_BT/nm^2) of an aggregate, as a function of $f_A = N_A/(N_A+N_C)$ for the symmetric sheet in Figure 1. Here $\chi_{AC} = 0$.

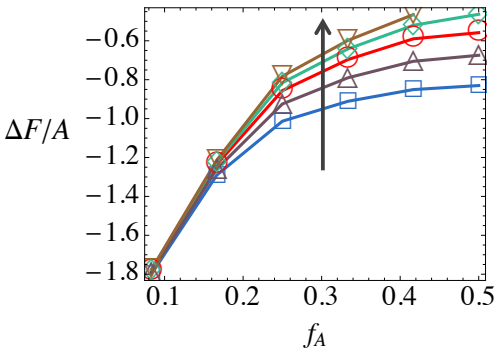

Fig. 4 Excess free energy per unit area $\Delta F/A$ (k_BT/nm^2) as a function of $f_A = N_A/(N_A+N_C)$ for a symmetric sheet in cartesian coordinates. Arrow indicates increasing $\chi_{AC} = 0, 1.0, 2.0, 2.75$, and 3.5.

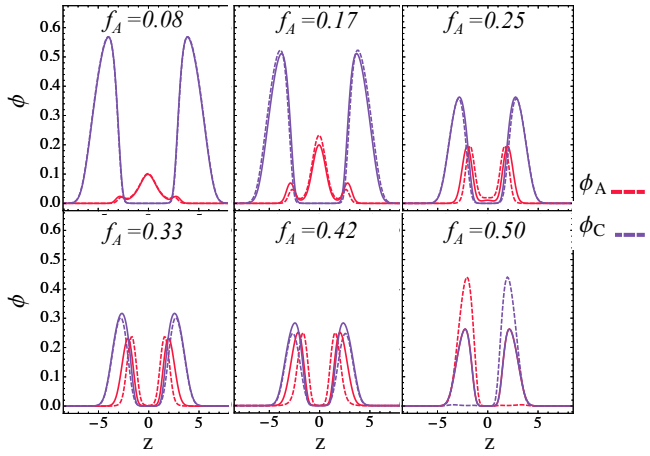

Fig. 5 Comparison of volume fraction profiles in the direction z (nm) normal to the sheet, for an ABC triblock with $\chi_{AC} = 0$ (solid) and $\chi_{AC} = 3.5$ (dashed).

by the majority solvophilic C block (purple, dotted). In particular, triblocks with $f_A = 0.08$ form bilayers with the A monomer species hidden within the solvophobic core, as depicted by the corresponding figure with a small peak in ϕ_A (red, solid) at the center. Triblocks with $f_A = 0.17$ form doubly mixed bilayers with three distinct peaks in ϕ_A, corresponding to positions at the center of the solvophobic core, and at the two interfaces with the solvophilic C density. The molecular packing arrangements for $f_A = 0.08$ and $f_A = 0.17$ are depicted schematically in Figures 1a and b, respectively, where the latter involves some molecules folding back on themselves. For $f_A > 0.17$, Figure 2 shows that the solvophilic A species is pushed out of the solvophobic core and towards the solvent interface, corresponding to a transition to a monolayer structure. The width of the monolayer, defined here as the peak–to–peak distance of ϕ_C, is notably smaller than the width of the bilayer. The monolayer is shown schematically in Figure 1c. Without an interaction incompatibility to drive the molecules to segregate (i.e. order), the monolayers possess a symmetric mixture of A and C blocks on both sides of the solvophobic core.

The field–theoretic free energy in eq. 2 may be separated into an energetic contribution given by the terms containing the interaction parameters χ_{JK} and κ_J, and an entropic contribution given by the single molecule partition functions, together with the term coupling the volume fraction field to its conjugate potential field. Thus, the competition between maximizing the configurational entropy within the aggregate and minimizing the unfavorable energetic interactions with the solvophobic core can be quantified. Figure 3 separates the enthalpic Δh (dashed) and entropic Δs (solid) contribution to the total excess free energy per unit area of the aggregate, relative to the bulk homogeneous solution. For $f_A \leq 0.17$, the system forms an aggregate that maximizes its entropy, at a (relatively) high energetic cost. These states correspond to the previously discussed bilayer, where the solvophilic monomers of the minority A species are buried within the solvophobic core. For $f_A > 0.17$, the system transitions to an aggregate that minimizes these unfavorable interactions, but at an entropic cost. These states correspond to the monolayer, where the A species has been expelled from the solvophobic core.

The sum of the entropic and enthalpic contributions gives the total excess free energy per unit area of the aggregate, relative to the homogeneous bulk solution. This quantity is shown in Figure 4 for $\chi_{AC} = 0$ (blue squares), as well as for $\chi_{AC} > 0$ (to be discussed in the following section). Here, $\Delta F/A$ increases with f_A, which, based on our discussion of Figure 3, is first an energetic and then an entropic effect. The latter indicates that the molecules in the monolayer become more aligned as the triblock becomes more symmetric, i.e., approaches $f_A = 0.5$.

3.2 Effect of interaction asymmetry, χ_{AC}

For all χ_{AC} considered, $\Delta F/A$ shown in Figure 4 increases with volume fraction f_A. However, for the bilayer structures ($f_A \leq 0.17$), $\Delta F/A$ is not very sensitive to the interaction parameter χ_{AC}, whereas for the monolayer structures ($f_A > 0.17$), $\Delta F/A$ clearly increases with increasing χ_{AC} (in the direction of the arrow). This observation can be understood by noting differences in the effects of increasing χ_{AC} to the volume fraction profiles of the bilayers and the monolayers.

Specifically, Figure 5 shows the volume fraction profiles of the hydrophilic A (red) and C (purple) species, compared at two different interaction parameters: $\chi_{AC} = 0$ (solid) and $\chi_{AC} = 3.5$ (dashed). For the bilayer with $f_A = 0.08$, there is a minimal overlap in ϕ_A and ϕ_C. Hence, the volume fraction profile is insensitive

to an increase in χ_{AC} (compare solid and dashed curves). However, for the doubly mixed bilayer with $f_A = 0.17$, there is a small overlap in ϕ_A and ϕ_C at the interface (solid) due to the molecules that have folded back on themselves, as illustrated schematically in Figure 1b. To minimize the unfavorable interactions between the A and C monomers upon increasing χ_{AC}, some of the folded molecules unfold, leading to a slight increase in ϕ_A at the center of the bilayer and a corresponding decrease in ϕ_A at the interface (dashed). In contrast, the more symmetric triblocks with $f_A > 0.17$ form mixed monolayers with a significant overlap in ϕ_A and ϕ_C (solid). By increasing the incompatibility between end blocks, the A block gets pushed closer to the interface *between* the B and C blocks (dashed), as it is no longer favorable for the A and C blocks to overlap, but the A block is still incompatible with the solvophobic B core. Having all the blocks in the ABC triblock terpolymer incompatible with each other results in a high interfacial tension for the mixed monolayer, corresponding to a significant increase in free energy per unit area with increasing χ_{AC}, as was shown in Figure 4. In fact, for $f_A = 0.5$, the mixed monolayer becomes unstable and the A species segregates to one side of the monolayer; see the dashed curves in Figure 5. Thus, it is possible to relieve these highly energetically unfavorable interactions by transitioning from a symmetric to an asymmetric monolayer. Of course, this comes with a loss in configurational entropy that corresponds with ordering the triblocks so that the A and C blocks are unmixed and only occur on separate sides of the solvophobic core.

4 Symmetric vs. asymmetric aggregates

In this section, we consider whether there are other cases where the symmetric monolayers are *metastable* (i.e. higher in free energy per molecule) relative to the asymmetric, unmixed monolayers. To obtain asymmetric solutions in a symmetric coordinate system, the SCFT equations are initiated with an asymmetric Gaussian distribution. Figure 6 shows the volume fraction profiles of the A and C blocks for $\chi_{AC} = 2$ (upper, solid) and $\chi_{AC} = 3.5$ (lower, dashed). For $\chi_{AC} = 2$, the unfavorable interactions between the two solvophilic end blocks starts to drive assemby into asymmetric monolayers for $f_A \geq 0.42$. For $f_A < 0.42$, the density overlap is not sufficient to drive end–block separation, and there is only one SCFT solution, corresponding to the previously–discussed symmetric (mixed) monolayer. For $f_A = 0.42$ the density overlap is sufficient to drive partial end–block separation, and for $f_A = 0.5$ the two solvophilic blocks show well–defined separation. Comparing the upper and lower rows in Figures 6, it can be seen that the triblocks with $\chi_{AC} = 3.5$ form asymmetric aggregates at lower f_A. Furthermore, for a given f_A, the separation in the A and C species is more defined at the higher χ_{AC}.

The excess free energy per molecule $\Delta F/n_p$ in the aggregates is plotted in Figure 7 for the two χ_{AC} values discussed in Figure 6, together with $\chi_{AC} = 0$. It can be seen that the bilayer to monolayer transition as a function of f_A corresponds to a decrease in $\Delta F/n_P$. The decrease is most notable for $\chi_{AC} = 0$ (blue squares), where the transition to mixed monolayers is not accompanied by an energetic cost due an overlap of incompatible end blocks. For $\chi_{AC} = 2$ (red), unmixing and separating the incompatible A, C end

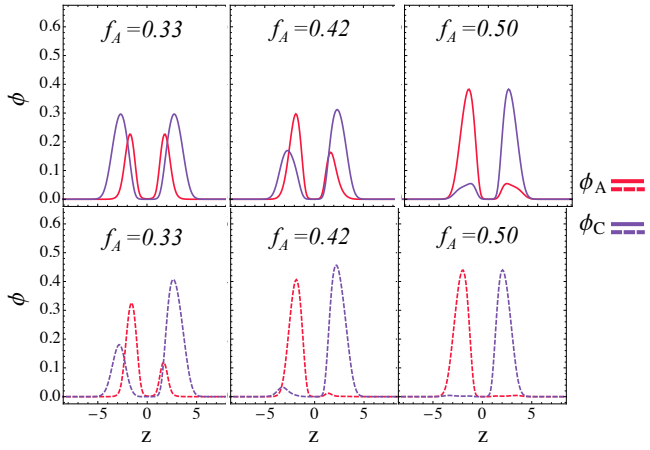

Fig. 6 Volume fraction profiles in the direction z (nm) normal to the sheet, for an ABC triblock with $\chi_{AC} = 2$ (upper, solid) and $\chi_{AC} = 3.5$ (lower, dashed).

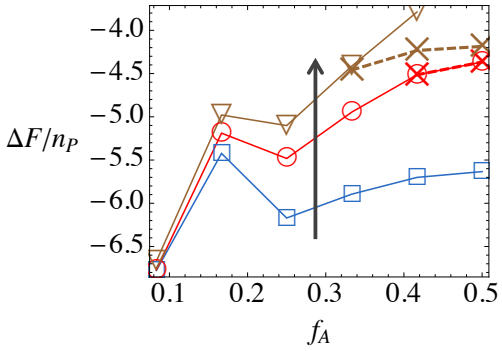

Fig. 7 Excess free energy (k_BT) per molecule $\Delta F/n_P$ as a function of $f_A = N_A/(N_A + N_C)$ for symmetric (solid) and asymmetric (dashed) sheets in cartesian coordinates. Arrow indicates increasing $\chi_{AC} = 0, 2.0,$ and 3.5.

blocks (dashed, $\times$) does not notably lower $\Delta F/n_P$; decreasing the unfavorable energetic interactions is offset by the loss in configurational entropy required to order the molecules. For $\chi_{AC} = 3.5$ (brown), the energetic interactions dominate the thermodynamics of assembly, leading to well-segregated monolayers (Figure 6, dashed) that are lower in free energy than the mixed monolayers.

Based on the aggregate with the lowest excess free energy per molecule $\Delta F/n_P$, we construct a phase diagram as a function of the degree of the asymmetry in the interaction χ_{AC} and architecture f_A between the solvophilic end blocks. The phase diagram includes the symmetric (mixed) bilayers and monolayers discussed previously, as well as the asymmetric monolayers observed in this section. We have checked that the spherical and worm-like micelles are not lower in free energy per molecule by comparing the aggregates in spherical and cylindrical coordinates with the aggregates in cartesian coordinates. The phase diagram shown in Figure 8 can be summarized as follows. For $f_A \leq 0.17$, the triblocks form symmetric bilayers at all values of χ_{AC}. Here, the minority A component is hidden in the solvophobic block of the bilayers, and increasing χ_{AC} does not have a qualitative effect on the structure of the bilayers. However, for $f_A > 0.17$, the

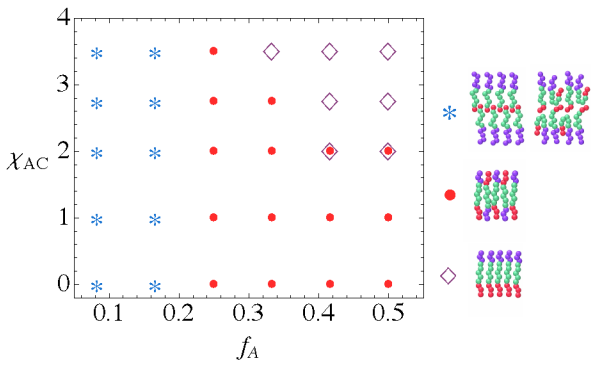

Fig. 8 Phase diagram as a function of interaction asymmetry χ_{AC} and molecular asymmetry f_A. Markers correspond to symmetric bilayer (stars), symmetric monolayer (circles), and asymmetric monolayer (diamonds).

triblocks form monolayers with a significant overlap in ϕ_A and ϕ_C. Thus, by increasing χ_{AC}, the monolayer transitions from symmetric to asymmetric, in which the A and C blocks separate to opposite sides of the solvophobic core. This transition requires a sufficiently high χ_{AC} and occurs at lower χ_{AC} for higher f_A, where there is more overlap in ϕ_A and ϕ_C. Note that the symmetric and asymmetric monolayers with $\chi_{AC} = 2$ have the same free energy per molecule (overlapping symbols in Figure 8).

Here we have explored the effect of χ_{AC} values from 0 to 3.5, which includes values less than and greater than the hydrophobic interaction strength. We note that a triblock terpolymer containing solvophilic end blocks with mutual incompatibility greater than that between the solvent and a solvophobic middle block would constitute an exceptional case. However, triblock–type peptide–polymer conjugates containing, for example, discrete solvophilic end blocks could constitute such a case. The hydrogen bonding patterns and electrostatic forces that often lead to complex interactions and secondary structures in peptides could lead to situations where two water-soluble peptide end blocks are extremely incompatible.[39] While the complexity of these interactions cannot be captured in our current calculations, we examine a wide range of interaction strengths with the aim of providing simplistic predictions of possible morphological variations in these chemically complex systems.

Finally, we have also considered concentration and solvent effects on the phase behavior. Not surprisingly, decreasing the polymer concentration stabilizes the micellar structures relative to the sheet–like structures, whereas increasing concentration leads to more stable sheets and, in some cases, multilamellar structures. In our open ensemble, where there is an infinite reservoir of molecules, these multilamellar structures expand to fill the computation box in the z direction, normal to the surface of the sheet. More interestingly, we have found that solvent effects may also yield similar multilamellar structures. By changing $\chi_{AS} = \chi_{CS} = 0$ to $\chi_{AS} = \chi_{CS} = 0.25$, the aggregates near the boundary between the symmetric bilayer (blue stars) and the symmetric monolayer (red circles) in Figure 8 become unstable. Here, expanding multilamellar structures arise because neither the bilayer nor the monolayer is stable and the system transitions between the two, each time doubling in number. This result can be understood by noting that the minority solvophilic A block is unstable at both the interface where there are solvents, and in the solvophobic core. Hence, the system transitions between the structure depicted schematically in Figure 1b, to one where the folded triblock molecules unfold the C (purple) block towards the center to form two symmetric (mixed) monolayers, as illustrated in Figure 1c.

5 Conclusions

Self-consistent field theory calculations demonstrate how the relative length $f_A = N_A/(N_A + N_C)$ and interaction strength χ_{AC} between the solvophilic end segments of an ABC triblock amphiphilic molecule may be used to control its assembly into mixed or segregated bilayers and monolayers. For increasing f_A, a transition from bilayers to doubly mixed bilayers to monolayers is observed. The preferred packing is dictated by competing entropic and enthalpic contributions, where the transition from bilayer to monolayer coincides with a decrease in the unfavorable interactions associated with exposing the solvophobic core to the minority solvophilic block, but at an entropic cost due to loss in configurational degrees of freedom of the triblocks. For the bilayers with negligible overlap in solvophilic blocks, increasing the interaction strength χ_{AC} has little effect on the packing mechanism and only symmetric, mixed bilayers are obtained. For the monolayers, sufficiently strong incompatibility is able to induce a transition to an ordered aggregate with an asymmetric distribution of end blocks across the two surfaces. Hence, by tuning the incompatibility between the end blocks of a triblock architecture, monolayer structures with tunable extents of segregation are achievable. These findings are summarized by the phase diagram in Figure 8.

Our results are expected to have significant implications in the development of functional symmetric and asymmetric nanostructures from amphiphilic molecules, which we are working to address. For example, vesicles prepared from synthetic amphiphiles can potentially simulate the asymmetric cytoplasmic membranes ubiquitous to cells, provided that the inner and outer surfaces of the vesicles present distinct chemical functionalities.[40,41] Indeed, synthetic bolaamphiphiles were originally inspired by natural analogues found in Archaea, in which the differential solubility of hydrophilic head groups was presumed to result in their segregation to opposite regions of a monolayer membrane.[42] Similarly, nanotubes prepared from synthetic amphiphiles have been proposed for capture and release technology; independent control of the inner and outer surface chemistry has been identified as a critical prerequisite enabling selective capture in the nanotube interior while ensuring nanotube compatibility when dispersed in a dissimilar material.[43]

6 Appendix

6.1 Calculation of the chain propagators for the discrete Gaussian chain

The chain propagators for the discrete Gaussian chain begin with the initial condition $q(\mathbf{r}, 1) = e^{-\nu\xi(\mathbf{r})}$ for placing the end monomer

at position $\mathbf{r}$. Propagating forward along the chain corresponds to moving to subsequent monomers $i+1$ in a stochastic process

$$q(\mathbf{r}, i+1) = e^{-\nu\xi} \int d\mathbf{r}' \Gamma(|\mathbf{r}-\mathbf{r}'|) q(\mathbf{r}', i), \tag{8}$$

where the Boltzmann weight depends on the species of monomer i and Γ denotes the conditional transition probability, assumed to be Gaussian.

Rather than attempt to solve eq. 8 exactly by integrating over all space, we recognize that, for a reasonably smooth external potential, the contributions from bond transitions for large $|\mathbf{r}-\mathbf{r}'|$ are vanishingly small so that they may be ignored. Together with the fact that eq. 8 is a Chapman–Kolmogorov equation, which can be converted in the continuum limit to a Fokker–Planck equation of the form [36]

$$\frac{\partial}{\partial s} q(\mathbf{r}, \mathbf{s}) = \frac{b^2}{6} \nabla^2 q(\mathbf{r}, s) - \nu\xi(\mathbf{r}) q(\mathbf{r}, s), \tag{9}$$

we can obtain the nearest-neighbor bond transition probabilities from a finite difference approximation of the spatial derivatives in eq. 9 (setting $\xi = 0$). The discretized version of eq. 8 becomes [37]

$$q(\mathbf{r}_j, i+1) = e^{-\nu\xi(\mathbf{r})} \sum_{\mathbf{r}_{j'}} \Gamma(\mathbf{r}_{j'} \to \mathbf{r}_j) q(\mathbf{r}_{j'}, i), \tag{10}$$

where it is understood that the summation is restricted to nearest neighbors of $\mathbf{r}_j$. For our 1D cartesian system, a space-centered finite difference approximation results in transition probabilities defined by

$$\Gamma(z_{j-1} \to z_j) = \Gamma(z_{j+1} \to z_j) = b^2/6h^2, \tag{11}$$

and a "survival probability" given by

$$\Gamma(z_j \to z_j) = 1 - 2(b^2/6h^2). \tag{12}$$

Here, j is the grid index and h is the grid spacing.

The above approach can be generalized to any geometry and more sophisticated finite difference approximations. We note that the finite difference scheme used here assumes that the range of a bond joining two monomers is on the order of (or less than) the grid spacing h. This requirement usually requires taking very small step sizes; in the field free case, the stability condition is $b^2 < 3h^2$. For cases where we wish to lengthen the range of the bonds, we can include next-nearest neighbor transitions (and beyond) by inserting n fictitious monomers at intermediate positions. These fictitious monomers satisfy eq. 10, but without the Boltzmann weight associated with the external field. For our case, we use $h = 1/5b$, with $n = 10$ fictitious beads. Finally, note that the discrete Gaussian chain given here, unlike the continuous Gaussian chain model, has finite range of bond lengths, which are specified by the grid spacing h and the number of fictitious beads.

7 Acknowledgement

Sandia National Laboratories is a multi-program laboratory operated by Sandia Corporation, a wholly owned subsidiary of Lockheed Martin Company, for the U.S. Department of Energy's National Nuclear Security Administration under contract DE-AC04-94AL85000. CLT is thankful for support from the Harry S. Truman Fellowship in National Security Science and Engineering. Research of BHJ, EDS, and MJS supported by the U.S. Department of Energy (DOE), Office of Science, Basic Energy Sciences (BES), Division of Materials Sciences and Engineering. ALF acknowledges support from the Sandia Laboratory Directed Research and Development (LDRD) program.

References

1 C. Sanchez, C. Boissière, D. Grosso, C. Laberty and L. Nicole, *Chem. Mater.*, 2008, **20**, 682–737.
2 Y. Shi, Y. Wan and D. Zhao, *Chem. Soc. Rev.*, 2011, **40**, 3854–3878.
3 L. Vaisman, D. H. Wagner and G. Marom, *Adv. Colloid Interf. Sci.*, 2006, **128–130**, 37–46.
4 S. Mourdikoudis and L. M. Liz-Marzán, *Chem. Mater.*, 2013, **25**, 1465–1476.
5 V. P. Torchilin, *J. Control. Release*, 2001, **73**, 137–172.
6 J. A. Hanson, C. B. Chang, S. M. Graves, Z. Li, T. G. T. G. Mason and T. J. Deming, *Nature*, 2008, **455**, 85–88.
7 J. N. Israelachvili, *Intermolecular and Surface Forces*, Academic, New York, 1992.
8 J.-H. Fuhrhop and T. Wang, *Chem. Rev.*, 2004, **104**, 2901–2937.
9 G. Riess, *Prof. Polym. Sci.*, 2003, **28**, 1107–1170.
10 I. W. Wyman and G. Liu, *Polymer*, 2013, **54**, 1950–1978.
11 P. Alexandridis, J. F. Holzwarth and T. A. Hatton, *Macromolecules*, 1994, **27**, 2414–2425.
12 P. Alexandridis and T. A. Hatton, *Colloid. Surf. A*, 1995, **96**, 1–46.
13 A. V. Kabanov, P. Lemieux, S. Vinogradov and V. Alakhov, *Adv. Drug Deliv. Rev.*, 2002, **54**, 223–233.
14 M. L. Adams, A. Lavasanifar and G. S. Kwon, *J. Pharm. Sci.*, 2003, **92**, 1343–1355.
15 R. Ni and Y. Chau, *J. Am. Chem. Soc.*, 2014, **136**, 17902–17905.
16 J. Grumelard, A. Taubert and W. Meier, *Chem. Comm.*, 2004, 1432–1463.
17 L. Wang, H. Huang and T. He, *Macromol. Rapid Commun.*, 2014, **35**, 1387–1396.
18 R. Stoenescu and W. Meier, *Chem. Comm.*, 2002, 3016–3017.
19 A. Blanazs, M. Massignani, G. Battaglia, S. P. Armes and A. J. Ryan, *Adv. Funct. Mater.*, 2009, **19**, 2906–2914.
20 H. Schlaad, L. You, R. Sigel, B. Smarsly, M. Heydenreich, A. Mantion and A. Mašić, *Chem. Comm.*, 2009, 1478–1580.
21 G. Njikang, I. C. M. Kwan, G. Wu and G. Liu, *Polymer*, 2009, **50**, 5262–5267.
22 N. Dan and S. A. Safran, *Macromolecules.*, 1994, **27**, 5766–5772.
23 L. Luo and A. Eisenberg, *Angew. Chem. Int. Ed.*, 2002, **41**, 1001–1004.
24 O. Terreau, L. Luo and A. Eisenberg, *Langmuir*, 2003, **19**, 5601–5607.
25 Y. Jiang, T. Chen, F. Ye, H. Liang and A.-C. Shi, *Macro-*

molecules, 2005, **38**, 6710–6717.
26 Y. Zhuang, J. Lin, L. Wang and L. Zhang, *J. Phys. Chem. B*, 2009, **113**, 1906–1913.
27 Y. Han, J. Cui and W. Jiang, *J. Phys. Chem. B*, 2012, **116**, 9208–9214.
28 J. Cui, Y. Han and W. Jiang, *Langmuir*, 2014, **30**, 9219–9227.
29 C. Gonzato, M. Semsarilar, E. R. Jones, F. Li, G. J. P. Krooshof, P. Wyman, O. O. Mykhaylyk, R. Tuinier and S. P. Armes, *J. Am. Achem. Soc.*, 2014, **136**, 11100–11106.
30 J. Cui and W. Jiang, *Langmuir*, 2010, **26**, 13672–13676.
31 M. Monzen, T. Kawakatsu, M. Doi and R. Hasegawa, *Computational and Theoretical Polymer Science*, 2000, **10**, 275–280.
32 J. Zhu, Y. Jiang, H. Liang and W. Jiang, *J. Phys. Chem. B*, 2005, **109**, 8619–8625.
33 C. Cai, L. Zhang, J. Lin and L. Wang, *J. Phys. Chem. B*, 2008, **112**, 12666–12673.
34 R. Wang, P. Tang, F. Qiu and Y. Yang, *J. Phys. Chem. B*, 2005, **109**, 17120–17127.
35 K. A. Dill, S. Bromberg, K. Yue, K. M. Fiebig, D. P. Yee, P. D. Thomas and H. S. Chan, *Protein Science*, 1995, **4**, 461–602.
36 G. H. Fredrickson, *The Equilibrium Theory of Inhomogeneous Polymers*, Oxford University Press, Oxford, 2006.
37 C. L. Ting and Z.-G. Wang, *Biophys. J.*, 2011, **5**, 1288–1297.
38 K. M. Hong and J. Noolandi, *Macromolecules*, 1980, **13**, 964–969.
39 A. R. Rodriguez, U.-J. Choe, D. T. Kamei and T. J. Deming, *Macromolecular Bioscience*, 2012, **2**, 805–811.
40 H.-T. Cheng, Megha and E. London, *J. Biol. Chem.*, 2009, **284**, 6079–6092.
41 D. L. Richmond, E. M. Schmid, S. Martens, J. C. Stachowiak, N. Liska and D. A. Fletcher, *Proc. Nat. Acad. Sci.*, 2011, **108**, 9431–9436.
42 J.-F. Fuhrhop and D. Fritsch, *Acc. Chem. Res.*, 1986, **19**, 130–137.
43 N. Kameta, H. Minamikawa and M. Masuda, *Soft Matter*, 2011, **7**, 4539–4561.